

# Site testing for the Discovery Channel Telescope

Thomas A. Bida<sup>a</sup>, Edward W. Dunham<sup>a</sup>, Leonard P. Bright<sup>a</sup>, Charles Corson<sup>b</sup>

<sup>a</sup>Lowell Observatory, 1400 W. Mars Hill Rd., Flagstaff, AZ, USA 86001

<sup>b</sup>National Optical Astronomy Observatories, 950 N Cherry Ave Tucson, AZ, USA 85719

## ABSTRACT

We present results of an extended campaign to test astronomical and environmental qualities of the intended site for the Discovery Channel Telescope, located at 2361m elevation near Happy Jack, AZ. A semi-permanent test station has been in operation since January 2003, consisting of a Differential Image Motion Measurement (DIMM) system and a weather station. Median seeing derived from DIMM measurements for January 2003 – May 2004 on 117 separate nights was 0.84 arcsec, with a first-quartile average of 0.62 arcsec. A wind sensor array deployed on a 12.2m tower is used to characterize air flow over the site. We find that ground induced turbulence becomes more prevalent below the 7.3m level. The Lowell DIMM system has also been run adjacent to the WIYN telescope for simultaneous comparative seeing measurements. Absolute correlations of DIMM seeing with WIYN image quality were good over two nights' observing under a range of environmental conditions.

## 1. INTRODUCTION

In summer 2001 Lowell Observatory conducted a limited astronomical site testing campaign in Northern Arizona to determine if local sites suitable for long-term operation of a new technology telescope could be identified. During this campaign, a portable Differential Image Motion Measurement (DIMM) system was operated sequentially on 30 evenings at several mountaintop sites within 75km of Flagstaff, with simultaneous comparative DIMM observations made at the Lowell Observatory's Anderson Mesa telescope site. The results of this initial survey indicated that good seeing conditions could be realized on a cinder cone located at 2361m elevation near Happy Jack, Arizona, approximately 65km SE of Flagstaff. In fall 2002 a semi-permanent site testing station was installed at the Happy Jack site, consisting of a DIMM system built around a Celestron 14-inch Schmidt-Cassegrain telescope and Photometrics CCD camera, and a standard weather station expanded with a 8-element wind sensor array. The site layout is pictured in Figure 1.

## 2. DIMM SYSTEM

The site-testing station consists of a Celestron 14-inch Schmidt-Cassegrain telescope mounted on a surface cement pier, housed in a roll-away shed with an adjacent trailer housing the system computers. The telescope aperture is at approximately 2.5m height above grade. Differential image motion is measured by use of a two-subaperture mask mounted on the telescope entrance aperture with a CaF<sub>2</sub> beam-deviating wedge mounted over one subaperture. The subaperture size is 8.9cm, separated by 25cm, and the wedge deviates one beam approximately 30 arcsec. The camera system is one of four identical instruments developed by a collaboration of investigators at NASA Ames, Lowell Observatory, MIT, and the University of Arizona, for stellar occultation photometry using the KAO, and fixed and portable ground-based telescopes<sup>1</sup>. Called Portable CCD (PCCD), it controls a liquid-cooled Photometrics CH250 camera head with Thomson 7883 front-illuminated CCD and associated timing electronics. The computer interface is composed of a 486-type PC, a National Instruments PC-TIO-10 timing board, and a TRAK GPS receiver. Reimaging 3:1 optics produce a plate scale of 0.4 arcsec/pixel at camera focus. The system contains a 10-position filter wheel mounted in a parallel beam, however, CCD seeing images are taken unfiltered. For seeing measurements, the CCD is read out in strip-scan mode by triggering off the GPS, binning 20 rows and serial shifting at a 10ms frame rate for 20s, resulting in 2000-row scan images. Strip-scans with the above optical setup have been acquired as fast as 7ms for test purposes, but we find that 10ms is sufficiently fast for the HJ site. Image acquisition frequency is normally 3 strip scans in direct sequence started on 5m intervals.

The strip-scan images are processed to derive the variance in image motion in the longitudinal direction between the apertures. Peaks of the two strips in each row are located, centroided, and statistically filtered to remove deviants in

separation, flux ratio, and saturated strips; row rejections typically total less than 5% of each stripscan. Following Sarazin and Roddier<sup>2</sup>, the variance in differential motion parallel to the line separating the subapertures (longitudinal) is

$$\sigma^2 = 2\lambda^2 r_0^{-5/3} [0.179D^{-1/3} - 0.097d^{-1/3}] \quad (1)$$

where  $D$  is the aperture diameter,  $d$  the separation between apertures,  $\lambda$  the effective wavelength of sensitivity of the system, and  $r_0$  the Fried seeing parameter<sup>3</sup>. The latter parameter is related to long-exposure FWHM (full width half maximum) of a point source by a telescope by the relation<sup>2</sup>

$$\text{FWHM} = 0.98\lambda / r_0 \quad (2)$$



Figure 1. The Happy Jack, AZ astronomical site test station overlooking the Mogollon rim and Verde River valley.

The result for our system thus represents the average seeing over the 20s interval of each stripscan. Our calculations assume an effective wavelength of  $0.7 \mu\text{m}$ , where the CCD responsivity is near maximum. Finally, the FWHM result is corrected for airmass by division by  $(\cos\gamma^{5/3})$ , where  $\gamma$  is the zenith distance angle. The seeing measurement limit for our system can be approximately defined by where  $r_0$  is equal to the distance between the outer edges of the subapertures, 33.9cm, corresponding to a FWHM of 0.42 arcsec.

Two examples of stable high-quality seeing observed at the site are shown in Figure 2; note that the measurements on 030920 (in UT YYMMDD format) reach the saturation limit of 0.42 arcsec. The cumulative seeing distribution for 458 hrs of observations at Happy Jack from January 2003-May 2004 is shown in Figure 3. The median seeing value is 0.84 arcsec, the most frequent binned measurement is 0.75 arcsec, with a first-quartile average of 0.62 arcsec. With simultaneous weather data acquisition, we compare environmental conditions with seeing in the next section.

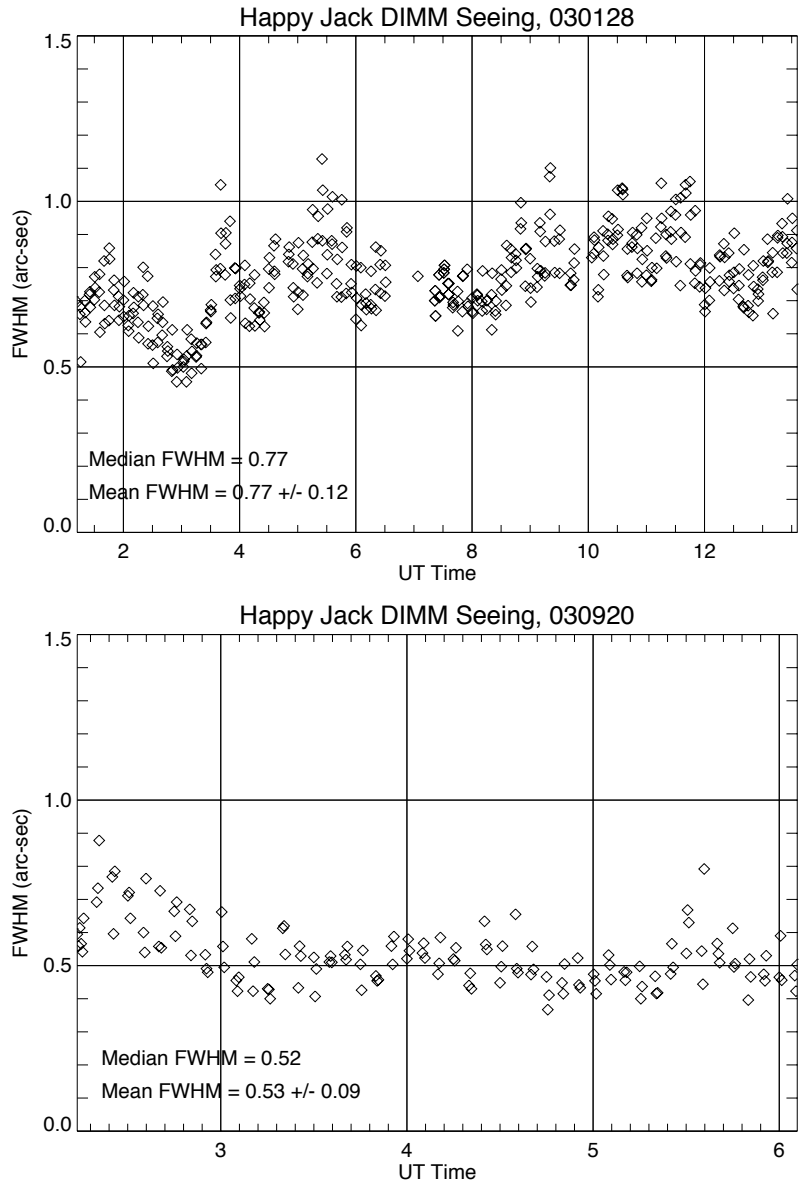


Figure 2. Time-series of DIMM seeing measurements for two dates (YYMMDD) at the Happy Jack site.

### 3. HAPPY JACK SITE ENVIRONMENT

The weather station consists of a programmable datalogger and combined temperature-relative humidity sensor both manufactured by Campbell Scientific, a barometric pressure sensor, five combined wind speed and direction sensors, and three vertical wind propellers. Data are sampled on 10s intervals, average values logged on 5m intervals, and peak wind gusts over the latter interval are also logged. Post-processing of the database includes use of a sunrise/sunset ephemeris to delineate day and night-time periods for all sampled days. Statistics are compiled, including mean, median, standard deviation, and peak values of the total and partial (80 and 90%) populations.

The site night-time temperature distribution is shown in Figure 4, and is found to be quite broad and bimodal, though moderate in extremes. The temperature-dewpoint spread has been less than or equal to 2 °C 17% of the sampled time

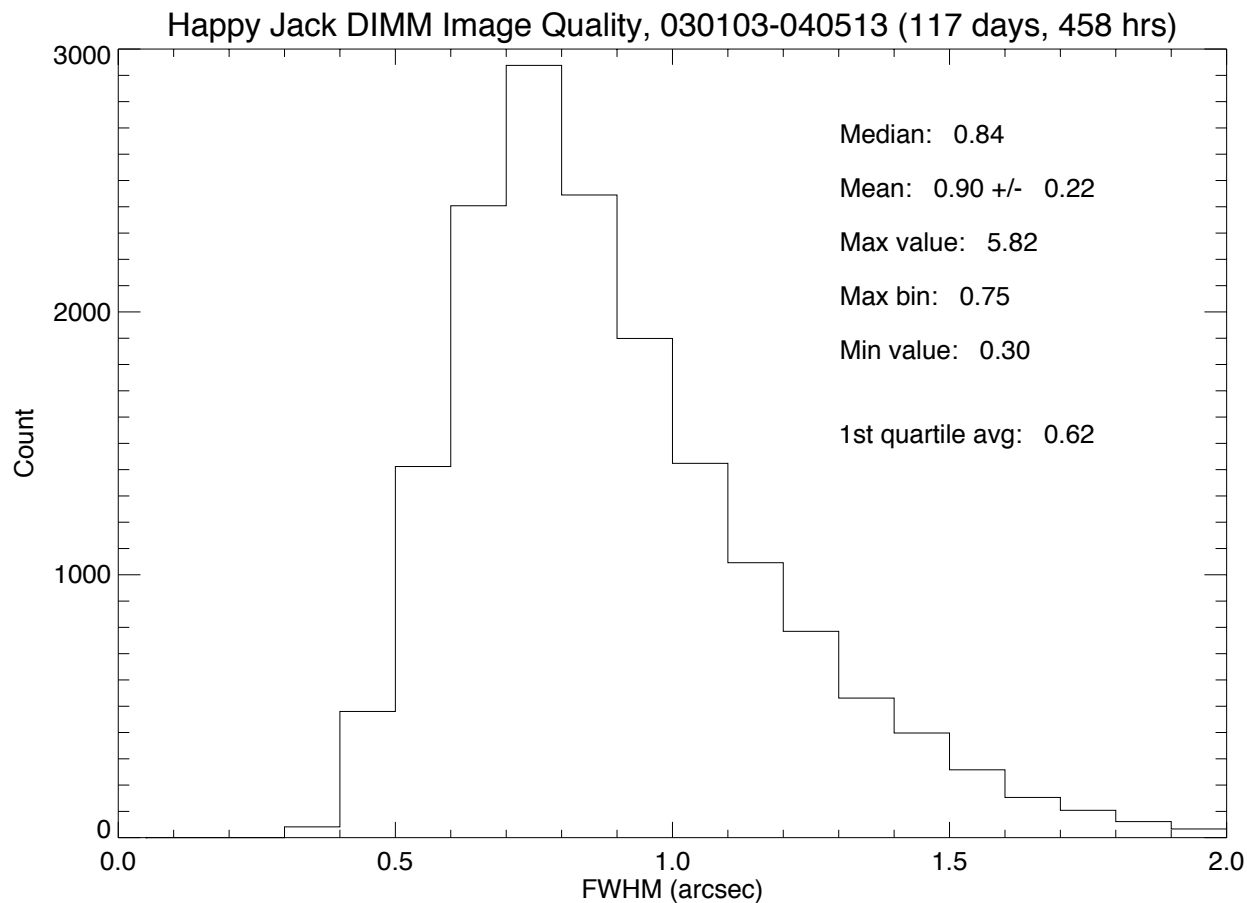


Figure 3. Cumulative seeing histogram for DIMM measurements at the Happy Jack site, from 030103-040330.

overall. Night-time temperature gradients are greatest in evening twilight; the median value to 1hr post-sunset is  $-1.4$   $^{\circ}\text{C}/\text{hr}$ . The temperature data can be compared with that recorded at the nearby US Forest Service Happy Jack Ranger Station<sup>4</sup>, approximately 1.5km E and 80m lower in elevation from our site. Measured daily low temperatures at the telescope site are approximately  $5$   $^{\circ}\text{C}$  higher on average than 30yr averages measured at the ranger station; daily high temperatures do not deviate as significantly to that long-term database. The difference in low temperatures will be verified by direct daily comparisons, however, this result is not surprising given that the ranger station is located in a shallow sink on the surrounding plateau, surrounded by tree cover which would be expected to quell circulation during cold night-time periods.

From January to July 2003 two combination wind speed and direction sensors were deployed on a 6.7m mast, at heights of 2.4m and 4.9m. From 15 August 2003 to present five sensors have been deployed at approximate heights of (2.4, 4.9, 7.3, 9.8, 11.6m) on a 12.2m tower. Three vertical propellers at the 4.9, 7.3, and 11.6m levels also were installed at the later time. The night-time wind distribution at 9.8m height is displayed as a wind rose in Figure 5. The site at this level is characterized by steady winds greater than 2.2 m/s (5 mph) 87% of the time, with the median direction out of the SW at 222 degrees. The mean gust-average velocity difference is 1.6 m/s at 9.8m. In order to estimate wind speeds at the design height of 27m of the DCT dome, the measured average wind with height is extrapolated from both linear (velocity vs. height) and logarithmic ( $\ln(z)$  vs. velocity) relationships, as shown in Figure 6. Lower boundary layer winds typically vary<sup>5</sup> as  $\ln(z)$ , however, our sample shows an increase in velocity at 11.6m and 2.4m over that relationship. A conservative estimate of velocity at dome height was then found by  $\ln(z)$  extrapolation from average velocities of the middle three levels from 4.9-9.8m. The upper bound was found by projection from the linear fit to full mast average velocity vs. height.

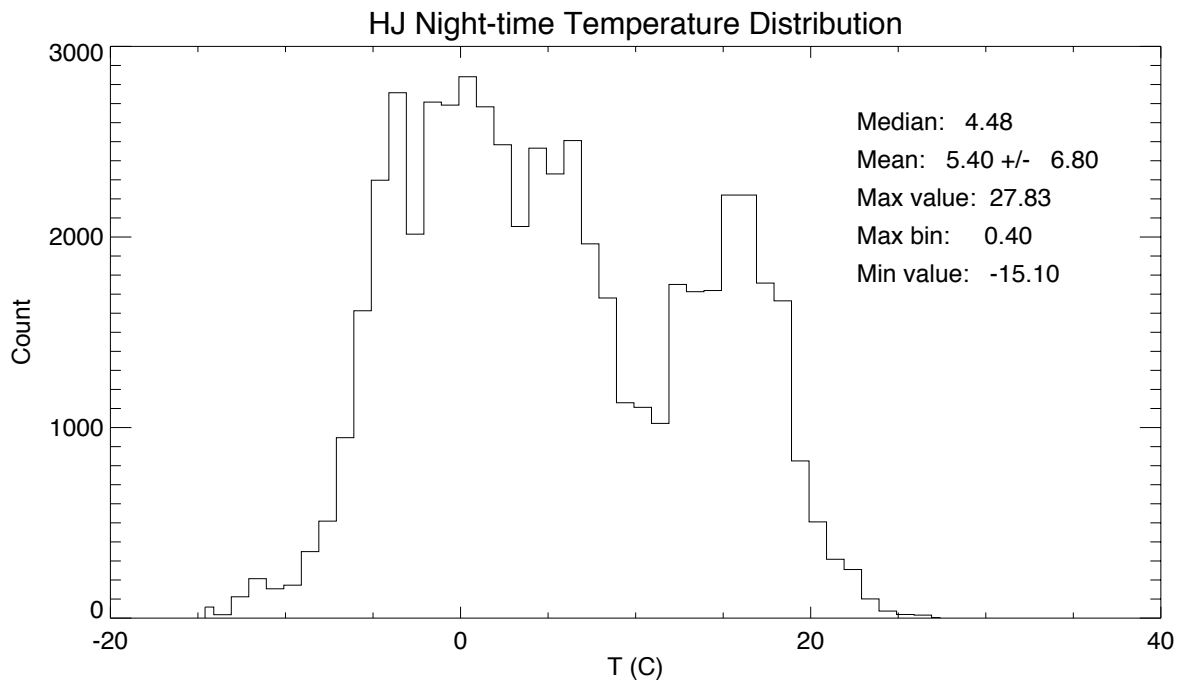


Figure 4. Night-time temperature distribution for the Happy Jack site.

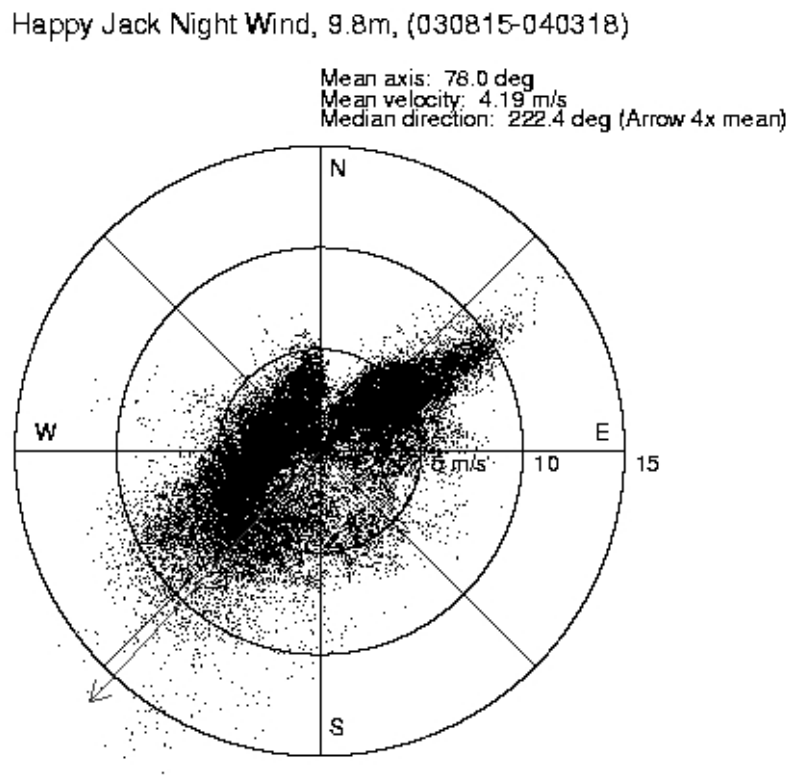


Figure 5. Night-time wind distribution at 9.8m height at the Happy Jack site.

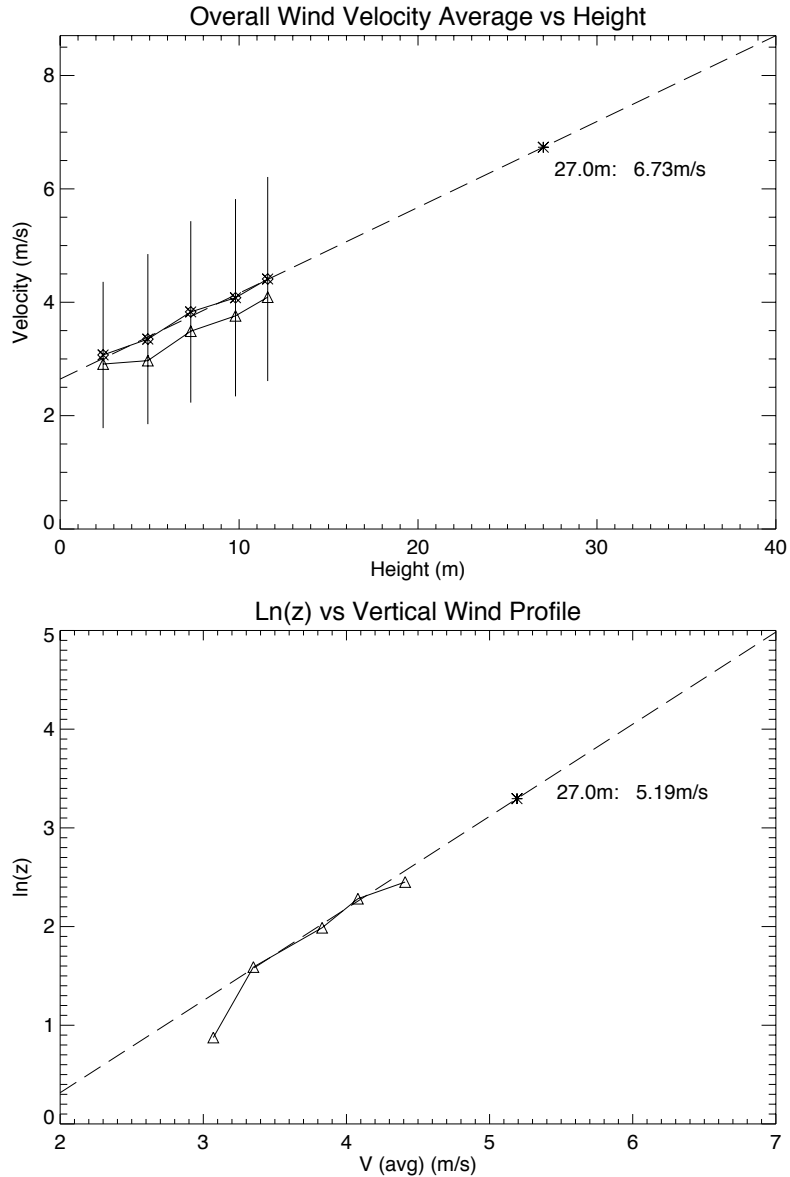


Figure 6. Measured wind velocity profiles. Upper plot: Averages, standard deviation bars, and median values (triangles) of measured winds vs. height. The dashed line is a linear extrapolation, with 30m value highlighted. Lower plot: Ln(height) vs. average wind velocity. The dashed line is a ln(z) extrapolation from the middle three values.

The wind velocity and direction readings at the 5 measurement heights along the mast have been cross-correlated to find the height where turbulence may reach a minimum, as guidance in determining a minimum height of the telescope pier. Correlation results are summarized in Tables I (velocity) and II (direction). Between adjacent sensors (along the diagonal of Table I), velocity correlations are strong, and dispersion ( $\sigma$ ) from linearity is low. These properties hold between the 11.6m height and individually the next two lower heights at 9.8m and 7.3m (column 2 of Table I) as well. However, both the correlation coefficient and the scatter from linearity increases abruptly in cross-correlation of the 11.6m and 4.9m measurements. Figure 7 shows correlations between the top sensor at 11.6m and those at 9.8m and 4.9m. The divergence in correlation at higher velocities is marked when the 11.6m velocity data is compared with that at 4.9m, versus the more linear relationship between 11.6m and 9.8m. This is an indication of increased boundary layer turbulence at 4.9m, over that measured at succeeding heights.

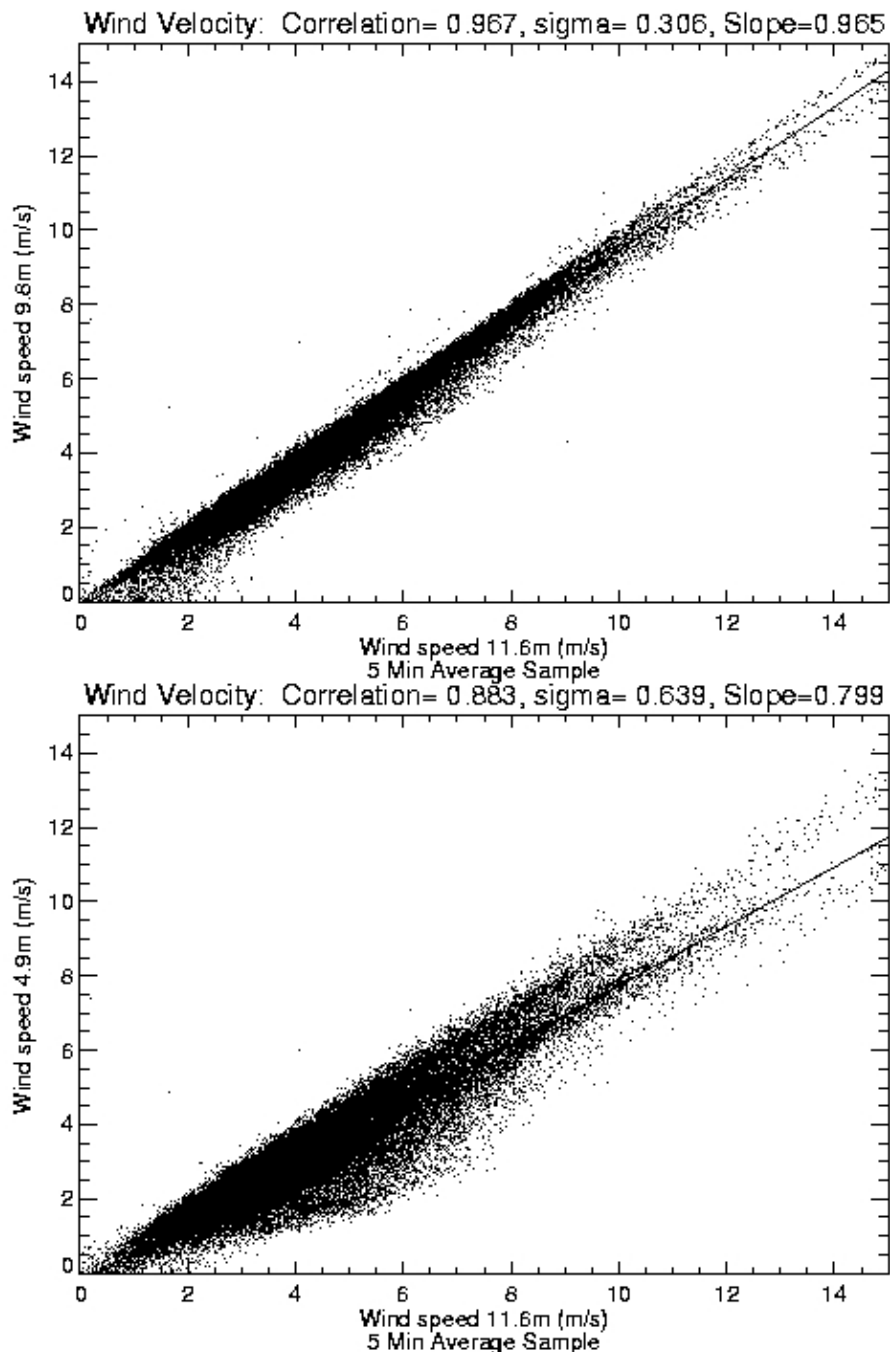


Figure 7. Cross-correlations of measured velocities at 11.6m and 9.8m (upper plot), and 4.9m (lower plot).

The wind direction sensor data set contained a small percentage (approximately 4% per sensor) of spurious readings and several sensors displayed extended deadband gaps ( $20^\circ$ ), so direction correlations were calculated after rejection of the outlying data points and overlapping gap regions. Wind direction correlations (Table II) are seen to be very high along the entire 11.6m mast, consistent with our experience that the vanes always point the same direction on average. The dispersion from linearity between adjacent sensors increases from top to bottom ( $\sigma$  diagonal, Table II), however, indicating that natural and facility-induced turbulence generates more small-amplitude oscillation in the wind direction near ground level.

**Table I. Wind Velocity Correlations**

	$C_v (\sigma \text{ (m/s)})$			
	1 (11.6m)	2 (9.8m)	3 (7.3m)	4 (4.9m)
1 (11.6m)	1.0			
2 (9.8m)	0.967 (0.31)	1.0		
3 (7.3m)	0.940 (0.39)	0.958 (0.22)	1.0	
4 (4.9m)	0.883 (0.64)	0.913 (0.45)	0.944 (0.29)	1.0
5 (2.4m)				0.964 <sup>a</sup>

a. Limited sample at 2.4m.

**Table II. Wind Direction Correlations**

	$C_d (\sigma \text{ (deg)})$			
	1 (11.6m)	2 (9.8m)	3 (7.3m)	4 (4.9m)
1 (11.6m)	1.0			
2 (9.8m)	0.998 (6.4)	1.0		
3 (7.3m)	0.996 (9.1)	0.996 (8.8)	1.0	
4 (4.9m)	0.997 (7.4)	0.994 (10.6)	0.990 (13.2)	1.0
5 (2.4m)				0.980 (11.0)

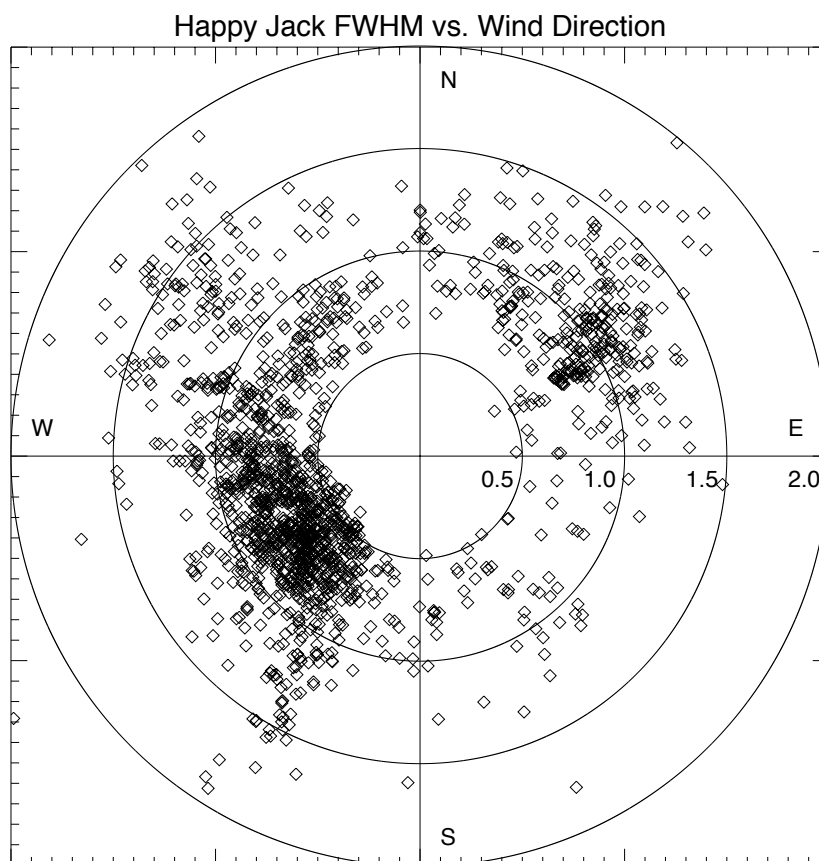


Figure 8. Cumulative DIMM seeing vs. wind direction, 15m averages; 0.5 arcsec seeing circle steps.



The DIMM seeing and environmental data sets are combined to examine the dependence of image quality on site conditions. Each of the seeing and environmental data sets are temporally binned into a common DOY timescale on 0.01d (0.24h) intervals, and then averaged over this interval. Sampled seeing is mostly flat compared against temperature, with only the lowest and highest temperature intervals displaying a deviation in seeing, as may be expected. Similarly, the seeing has had little correlation with the temperature-dewpoint spread. These results are indicative of a dry atmosphere with a threshold above which most clear climatic conditions produce consistent seeing.

Wind velocity does affect seeing in general, with the most consistent sub-arcsec seeing achieved when the wind is greater than about 2.5m/s and less than about 7m/s. The vertical wind component only appears to degrade seeing when largely downward. Winds out of the WSW also favor good seeing for our sample, as shown in Figure 8. As the site is clear of vegetation from SE through W, and the topography rapidly drops 140m over about 1 km to a lower plateau to the SW, the best observing conditions generally occur when the wind is from that prevailing direction. These findings are reasonable, as lower or higher winds from directions other than the prevailing wind encounter more obstacles and also imply a changing rather than steady-state atmosphere.

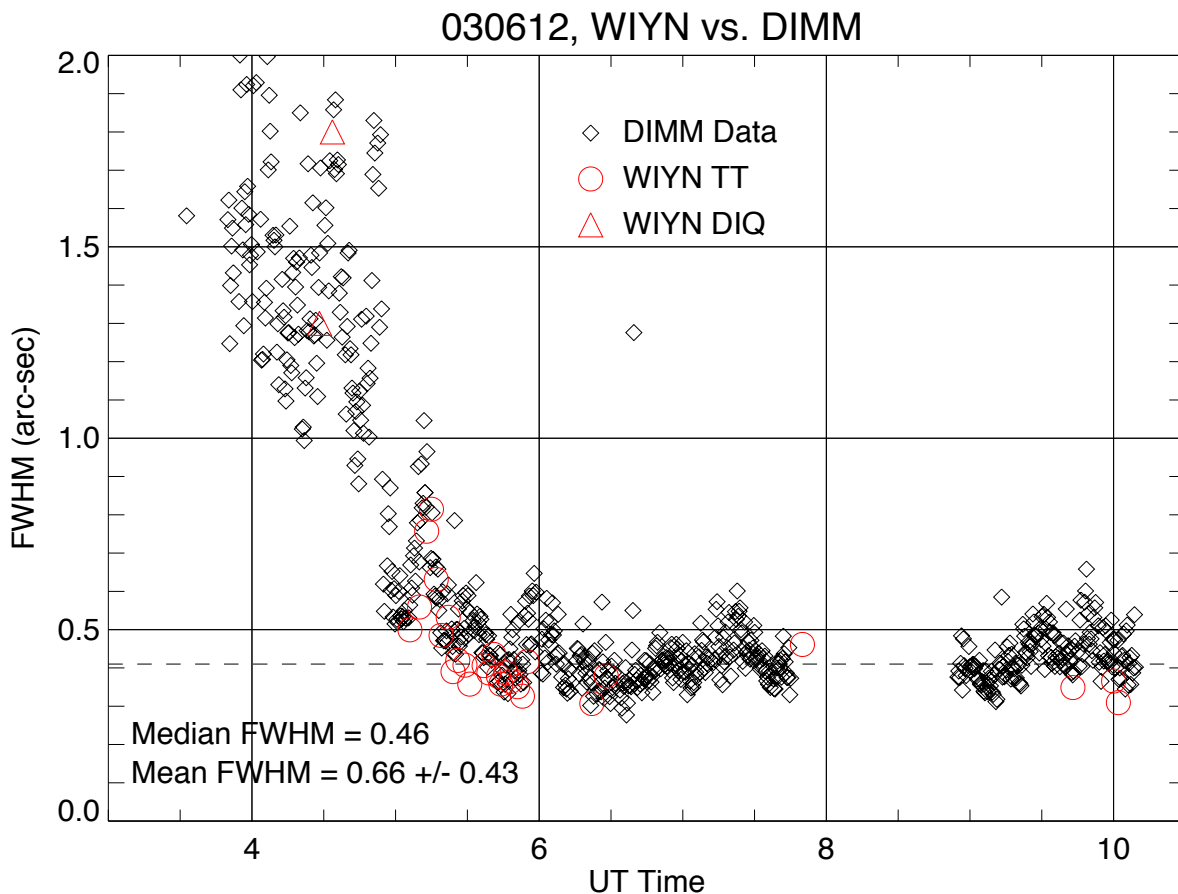


Figure 9. Lowell DIMM seeing vs. WIYN DIQ (delivered image quality camera) and WTTM measured image quality for 030612. The dashed line at 0.42 arcsec represents an approximate seeing saturation point for the DIMM system.

#### 4. DIMM-WIYN COMPARISON

In order to verify the calibration of the DIMM system used to characterize the DCT site, we were interested in cross-calibrating seeing measurements with a large telescope of well-known, high-quality imaging characteristics. The Lowell site test system was transported to Kitt Peak in June 2003 for a two-night run of DIMM observations in concert with the WIYN telescope<sup>6</sup>. The WIYN was configured with the WIYN Tip-Tilt Module (WTTM)<sup>7</sup> and imaging camera, which produces a plate scale of 0.1125 arcsec/pixel. The WTTM was run in engineering-test mode during both nights of our joint observations; most data compared with the DIMM results were taken in R-band at exposures of 10s with tip-tilt correction. The Lowell DIMM was set up on a cement pier approximately 20m W of the WIYN enclosure. Two nights' observations were conducted; the first (030611) was characterized by high winds and highly variable seeing, with both the WIYN telescope and the DIMM system impacted by wind buffeting. The second (030612) was more quiescent and fortuitously yielded long periods of consistently very good image quality. Figure 9 compares the 030612 DIMM and WIYN seeing measurements. That night began with variable winds and poor seeing, but improved rapidly to moderate prevailing wind from the W with excellent seeing. A turbulent fluctuation in the atmosphere occurred from 0500-0515 UT, significantly detected as an equivalent deterioration in both DIMM and WIYN measured image quality. Afterwards, the seeing converged to a well-compared steady state value of about 0.45 arcsec for the remainder of the night. The results from 030611 included additional seeing measurements between 0.6 and 1.2 arcsec over 3hrs time with moderate scatter, where the DIMM and WIYN derived seeing values also displayed good agreement. Based on these results, we are reasonably confident that the Lowell DIMM system is measuring seeing values that are representative of large telescope tip-tilt-corrected direct imaging observations.

#### 5. FUTURE WORK

We have conducted several measurements of sky brightness at the Happy Jack site by use of the Photometrics camera head with a fast stock camera lens. We aim to characterize the sky brightness in standard optical passbands from the zenith to cardinal points of interest including the Phoenix metropolitan area (160km distant), the Verde Valley in the Clarkdale area, and Flagstaff. We have also run a lunar scintillation measuring system near full moon on 20 nights in parallel with the DIMM system. The measurement of scintillation from an extended object<sup>8</sup> such as the sun or moon may be used to further probe atmospheric turbulence over a site. Our lunar scintillation system was custom-built at Lowell using a photomultiplier and associated electronics, with data acquired through a Keithley PCMCIA 16-bit ADC interface at 2kHz. Preliminary analysis of lunar scintillation data shows that RMS fluctuations in lunar irradiance do correlate well with variations in DIMM seeing measurements, though there are night-to-night offsets in the scintillation data. Such irradiance fluctuations reveal lower boundary-layer effects as witnessed in tests at ground vs. dome level at the Lowell 1.8m telescope at Anderson Mesa.

#### ACKNOWLEDGEMENTS

We thank Katie Morzinski and Mark Bielecki for their great efforts in the field during the 2001 site testing campaign, John DeDecker and Kelley Moore of Lowell Observatory for observing and analysis support early in the extended Happy Jack project, and Nat White of Lowell for installation of the telescope enclosure. We also thank Richard Green and John Glaspey of KPNO for supporting our tandem observations with the WIYN.

#### REFERENCES

1. Dunham, E.W., 'Optical instrumentation for airborne astronomy', *Airborne Astronomy Symposium on the Galactic Ecosystem, ASP Conference Series V. 73*, 517-522, 1995, M.R. Haas, J.A. Davidson, E.F. Erickson, Eds.
2. Sarazin, M. and F. Roddier, 'The ESO differential image motion monitor', *Astron. Astrophys.* 227, 294-300, 1990.
3. Fried, D.L., *JOSA* 55, 1427, 1965.

4. Western Regional Climate Center, Desert Research Institute, 2215 Raggio Parkway, Reno, NV 89512, [www.wrcc.dri.edu](http://www.wrcc.dri.edu).

5. Hess, S.L., *Introduction to Theoretical Meteorology*, p. 276-278, Holt and company, New York, NY, 1959.

6. Sawyer, D.G., Corson, C., Saha, and A. Saha, 'Optimizing the delivered image quality at the WIYN 3.5-m telescope', *Telescope Structures, Enclosures, Controls, Assembly/Integration, Validation, and Commissioning, Proc. SPIE V. 4004*, 2000, T. A. Sebring, Torben Andersen, Eds.

7. Claver, C.F., Corson, C., Gomez, R.R., Daly, P.N., Dryden, B. and B. Abereshi, 'WIYN Tip-Tilt Module performance', *Proc. SPIE 4837*, 438-447, 2003.

8. Beckers, J.M., 'On the relation between scintillation and seeing observations of extended objects', *Solar Physics* 1455, 399-402, 1993.